JMEPEG (2022) 31:9303–9317
https://doi.org/10.1007/s11665-022-06902-5

1059-9495/$19.00

TECHNICAL ARTICLE

Rapid Strengthening of Interstitial Free Steel Using Amorphous FeC Thin Films and Induction Heating

Elisa Cantergiani, Xavier Sauvage, Colin P. Scott, and Arnaud Weck

Submitted: 20 October 2021 / Revised: 23 February 2022 / Accepted: 6 March 2022 / Published online: 10 May 2022

A new process to rapidly obtain high-strength interstitial free (IF) steel was investigated. Thin sheets of IF steel were coated on one or both sides with an amorphous FeC film and subjected to a two-step induction heating cycle (1100 °C followed by an isothermal hold at 780 °C for 2 or 4 min) and a rapid quench in water. Tensile mechanical properties were measured, and a yield stress of 374 MPa and an ultimate tensile strength of 448 MPa were achieved after 2 min of induction heating. After 4 min of induction heating, the yield stress and the ultimate tensile strength drop at 206 and 320 MPa, respectively. During tensile testing, the specimens induction heated for 2 min show Lüdering, which is suppressed when the induction heating is extended to 4 min. Vickers microhardness measurements through thickness confirm that higher mechanical properties are obtained after 2 min of induction heating. Transmission electron microscopy reveals that strengthening results from dislocations, carbon in solid solution, and the precipitation of nanosized TiC particles. A fine microstructure with an average grain size of 15 μm is preserved after the induction heat treatment.

Keywords FeC films, induction heating, interstitial free (IF) steels, physical vapor deposition (PVD), transmission electron microscopy (TEM)

1. Introduction

A major effort in steel research is dedicated to strengthening of steels used for automotive applications to comply with more stringent requirements for fuel efficiency (Ref 1). Interstitial free (IF) steels and ultra-low-carbon (ULC) steels are both used for car body panels and packaging because of their low cost and good formability during conventional deep-drawing operations. The yield stress of ULC steels can be increased by only 50-60 MPa using bake hardening, while IF steels are in general not bake hardenable because the few carbon atoms present in the composition (≤ 30 ppm) are stabilized with Ti or Nb to form stable precipitates (Ref 2). IF steels are strengthened by adding manganese, silicon and phosphorus or by using grain refinement processes and high deformation through cold rolling (Ref 3, 4). Current commercial IF steels available for automotive applications have a maximum yield stress of 300 MPa with strain at fracture of 30% (Ref 5), while transformation-induced plasticity (TRIP) steels have yield stresses of 450-650 MPa and strain at fracture of 20-25% depending on the alloying element (Ref 6). New methods to strengthen IF steels by careful control of their composition (e.g., addition of copper or nitrogen) and subsequent heat treatment have been published (Ref 7, 8). The addition of 1.18 wt.% of copper increases the yield stress to 456 MPa but no value of strain at fracture has been mentioned (Ref 7). Nitriding of IF steel in a potassium nitrate salt bath can result in yield stresses ranging from 570 up to 1060 MPa depending on the nitriding time; however, the strain at fracture is below 10% (Ref 8).

Starting from this background, a new process to strengthen IF steel is proposed in this paper. The advantages of the method presented here are its high efficiency in terms of annealing time and that carbon is simply used as the strengthening element. Carbon is often introduced by careful control of steel composition or through a carburization treatment that requires several hours at temperatures close to 800 °C (Ref 9). In the present work, the carburization of IF steel was performed via the deposition of an amorphous FeC film followed by a rapid diffusion annealing heat treatment done through induction heating. In literature, electroplating (Ref 10, 11), hot filament chemical vapor deposition (HFCVD) (Ref 12) or electrophoretic deposition process (EPD) (Ref 13) are described as successful techniques to obtain nano- and microcoatings. More recently, solgel methods were used to obtain self-healing coatings on metallic substrate (Ref 14). However, in steel industries the physical vapor deposition (PVD) process is often implemented at industrial scale, for instance for zinc coating of

Elisa Cantergiani, Department of Mechanical Engineering, University of Ottawa, 161 Louis Pasteur, Ottawa, ON K1N 6N5, Canada; and Max-Planck Institut fuer Eisenforschung GmbH, Max-Planck Strasse 1, 40237 Düsseldorf, Germany; **Xavier Sauvage**, Groupe de Physique des Matériaux UMR CNRS 6634, Université de Rouen, BP-12, 76801 Saint Etienne du Rouvray Cedex, France; **Colin P. Scott**, Canmet MATERIALS, 183 Longwood Road S., Hamilton, ON L8P0A5, Canada; and ArcelorMittal Research SA, Maizières-lès-Metz F-57283, France; **Arnaud Weck**, Department of Mechanical Engineering, University of Ottawa, 161 Louis Pasteur, Ottawa, ON K1N 6N5, Canada; Department of Physics, University of Ottawa, 150 Louis Pasteur, Ottawa, ON K1N 6N5, Canada; and Centre for Research in Photonics at the University of Ottawa, 800 King Edward Ave., Ottawa, ON K1N 6N5, Canada. Contact e-mails: e.cantergiani@mpie.de aweck@uottawa.ca.

steel substrates to avoid atmospheric corrosion (Ref 15). PVD is considered to be a low-temperature (~ 250 °C) deposition technique with large flexibility for the production of multilayered coatings of variable compositions. The advantage of PVD is the accurate thickness control and the lower environmental impact compared to standard electrodeposition or hot-dip galvanizing processes (Ref 15, 16). Thus, PVD is a technique that can be available in steel industries and that potentially can be used to deposit the FeC film used in this investigation.

The main advantage of induction tempering over furnace tempering is the rapid heating rate that can be attained, which allows preserving fine grains microstructures in the steel substrate. Moreover, induction tempering can be integrated in industrial line production and it is already widely employed by automotive companies to temper hardened components such as shafts, bars or joints (Ref 17). Induction heating was used to study microstructure and mechanical property evolution in Fe-1.4%Cr-1%C pearlitic steels (Ref 18), and it is considered advantageous compared to other heating methods, because of its energy efficiency with shorter start-up and shut-down times. Furthermore, induction heating plants can be used with protective atmospheres in case oxidation of the parts has to be avoided (Ref 17).

The authors have already shown that amorphous FeC films can act as carbon reservoirs to diffuse a controlled amount of carbon in a coated IF substrate (Ref 19, 20). However, for this carbon diffused IF steel, the maximum yield stress was 300 MPa with a strain at fracture of 30% because at temperatures higher than 500 °C the amorphous FeC film crystallizes forming cementite (Fe_3C) limiting further carbon diffusion into IF substrate. Moreover, all tensile curves had Lüdering, which is in general undesirable for forming operations.

The work presented here has three main goals: The first is to maximize the strength of the coated IF steel by minimizing the time required to reach the isothermal temperature for carbon diffusion from FeC PVD films using induction heating. The second goal is to limit or suppress the formation of Lüder bands. The third goal is to demonstrate that this technique can be used to create graded steel sheets with a high hardness close to the coated surface and low hardness at the uncoated surface, which would be promising to obtain dent resistant steels while maintaining ductility.

2. Materials and Methods

2.1 Material and Induction Heat Treatment

The composition of the IF steel sheets used in this work contains 14×10^{-3} at.% of carbon, 64×10^{-3} at.% of titanium, 113×10^{-3} at.% of manganese, 22×10^{-3} at.% of sulfur, 16×10^{-3} at.% of phosphorus and 7×10^{-3} at.% of nitrogen and iron in balance. This chemical composition (provided by the producer) was obtained through a combination of optical emission spectroscopy (OES) for most elements and LECO combustion analysis for C, N, O, S.

The IF substrate has an amount of titanium 4.5 times higher (in wt.%) than the amount of carbon. This amount of titanium stabilizes the carbon and nitrogen present in the initial steel sheet. The sheets were 0.197-0.200 mm thick and were cut into subsize tensile samples using electro-discharge machining (EDM). Tensile samples had a dog-bone shape with a gauge length of 5 mm and a width of 1 mm (Fig. 1a). These tensile specimens were then cleaned using ethanol followed by etching with a 2 vol.% Nital solution and then rinsed with distilled water and ethanol before being coated either on a single side or on both sides with a 500 ± 20 nm thick amorphous FeC film containing 30 ± 3 at.% of carbon (balance Fe) using physical vapor deposition (Fig. 1b) following a procedure described in literature (Ref 20, 21). The coated specimens were then sealed under vacuum (10^{-6} Torr) in quartz cylinders and subjected to an induction heat treatment followed by quenching in water. Indeed, the presence of air is detrimental for the diffusion of carbon from FeC PVD films due to decarburization of the film (Ref 20). The quartz ampoule is inserted in a water-cooled copper coil which is connected to an alternate current (AC) generator whose power is varied to control the temperature experienced by the sample. Sample temperatures were measured using an infrared pyrometer, IGA 15 Plus, distributed by LumaSense technologies. During the heat treatment, an initial temperature of 1100 °C is reached with a heating rate of

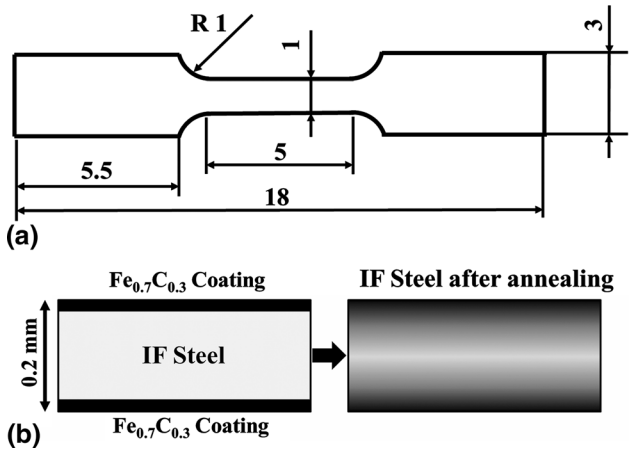

Fig. 1 (a) Dog-bone tensile sample (all dimensions are in mm), (b) schematic view of the thickness for IF steel double side coated before and after annealing

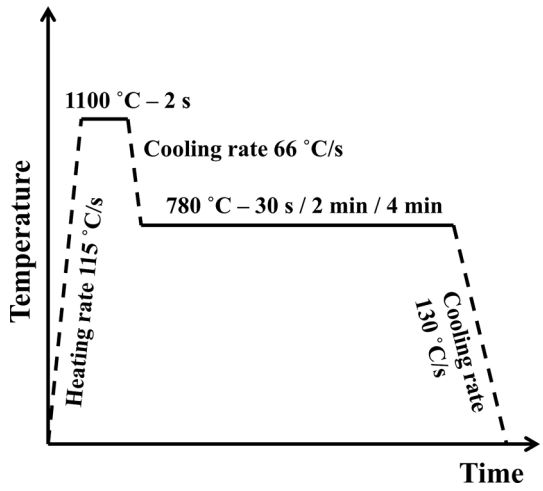

Fig. 2 Diagram for the induction heating treatment showing heating and cooling rate

115 °C/s and the coated steel is kept at this temperature for 2 s to fully austenitize the specimen. The temperature is then lowered to 780 °C and maintained for 30 s, 2 min or 4 min before quenching in water. Figure 2 shows a schematic diagram of the heat treatment profile. The same heat treatments were performed on uncoated (as received) IF steel to investigate the stability of the substrate during induction heating and to prove that no variation in mechanical properties came from the uncoated IF substrate. The induction heating process was selected because it allows reaching fast heating rates that cannot be obtained with standard vacuum furnaces using resistive elements. If the same heating cycle (1100 °C-2 s followed by holding at 780 °C for different times) would be applied to coated IF steel using standard heating furnaces, the heating to go from 25 to 1100 °C and the cooling rate to go from 1100 to 780 °C would be too slow and grain growth in the microstructure cannot be avoided. The fast heating rates obtained with induction heating prevent this grain growth and at the same time maximize carbon diffusion from the FeC film before it crystallizes. Thus, induction heating is selected for its high heating rates and the possibility to properly control the heating rate with precision.

The IF thin metal sheet is enclosed inside a coil where the alternate current (AC) flows. This alternate current flowing inside the coil produces a magnetic field which induces a current flow inside the metallic sheet. The current flows in opposite direction in the upper and lower sides of the metallic sheet. The thickness depth, where the current flows, is named skin depth (Ref 22). Joule heating of the metallic sheet is caused by these currents flowing in opposite direction. According to literature (Ref 22), if the sheet thickness is less than 4 times the skin depth, the currents at the upper and lower sides will extinguish each other. For thicknesses lower than 2.5 times the skin depth, the current is attenuated and Joule heating is no longer possible. The induction heating system used for these experiments has 200 kHz frequency while the resistivity of iron at 780 °C is 101×10^{-8} Ωm (Ref 23) and its magnetic permeability (μ) is 6.3×10^{-3} H/m. With these values, the calculated skin depth is 16 μm, while the total thickness of the sample is 197 μm, and thus, the skin depth is sufficiently small to guarantee Joule heating avoiding cancellation of the top and bottom face induced currents.

2.2 Mechanical Properties and Microstructure Analyses

A first set of induction-heated samples were tensile tested at a strain rate of 5×10^{-4} s^{-1} at room temperature, and engineering stress–strain curves were obtained. At least two samples for each condition were tested. When Lüdering was present, the upper yield stress was chosen (i.e., maximum stress before the start of Lüder's plateau), while if no plastic instability was detected, the yield stress was obtained as the stress corresponding to 0.2% engineering strain. Another set of specimens were induction heated with the same procedure, and after the treatment, they were cold mounted in resin and polished down to 0.05 μm using diamond solutions and colloidal silica for microhardness measurements. Hardness profiles through thickness were obtained from a Vickers microhardness tester applying a load of 25 g for 10 s. In literature (Ref 24), it was reported that quench age hardening can occur at temperatures of 35 °C for a time of 16×10^4 s of storage for aluminum-killed low-carbon steels quenched from 700 °C. However, in the present study quench-aging did not occur because some specimens were tested right after the induction heat treatment and others were stored at 15-20 °C in a dried environment and tested 3-4 days after the heat treatment. As the induction heat treatment was the same, and despite the storage time at 20 °C, all samples had the same mechanical properties and microstructure, indicating that no significant quench-aging occurred. This was verified for both double-coated and uncoated IF steel samples. The microstructure of the specimens was investigated after a light etch with a 4 vol.% Nital solution using optical microscopy and a scanning electron microscope (JSM-7500F FESEM (JEOL)). Transmission electron microscopy was used to assess dislocation density, density of precipitates and to identify the type of precipitates. Transmission electron microscopy (TEM) observations were carried out in scanning mode (STEM) using a JEOL ARM200F microscope operated at 200 kV. Bright-field (BF) images were recorded with collection angles up to 45 mrad. Elemental mapping was carried out using energy-dispersive x-ray spectroscopy (EDS) with an Oxford Instruments x-max detector (collection angle 0.7 sr). Thin foils samples were prepared by mechanical dimpling followed by ion milling or alternatively using a focused ion beam (FIB).

3. Results and Discussion

3.1 Microhardness Profiles

Figure 3 shows the results of Vickers microhardness tests where the hardness of the uncoated IF substrate remains unaffected after induction heat treatment (UC curves in Fig. 3). For each location through thickness, the plotted Vickers measurement is the average of 10 measurements (error bars in Fig. 3 represent the standard deviation). For single-side-coated samples, a large hardness gradient is observed after just 30 s of induction heating, (247 MPa at the coated surface, 161 MPa at the uncoated surface). After 2 min of induction heating, the double-sided sample shows the highest increase in hardness with a slight gradient (250 MPa at the center, 275 MPa at the surface), while after 4 min the hardness decreases (190 MPa at the center, 198 MPa at the surface).

The time for induction heat treatments was chosen based on the expected carbon profile through thickness both for double-side-coated and one-side-coated specimens. The carbon profile can be predicted using second Fick's law and considering a maximum amount of carbon of 0.065 at.% available for diffusion because of film crystallization. The amount of carbon that is available for diffusion into the IF substrate is limited by crystallization of the amorphous FeC film (Ref 25, 26). The crystallization temperature of FeC amorphous films depends on initial carbon content in the film (Ref 21, 27). X-ray diffraction measurements were performed on FeC films annealed in a high vacuum furnace (Ref 27) or annealed using induction heating (Fig. 4). For both heat treatments, the film was found to crystallize for temperatures equal to or above 530 °C. For diffusion annealing in vacuum furnaces, the FeC film forms mainly cementite (Fe_3C). Stoichiometric calculations show that only 0.0645 at.% of carbon is left available for diffusion into the IF substrate considering full crystallization of the film into cementite. Figure 4 shows the results of grazing x-ray diffraction performed on induction-heated FeC film. When the induction heating is only performed for 1 min, there is only

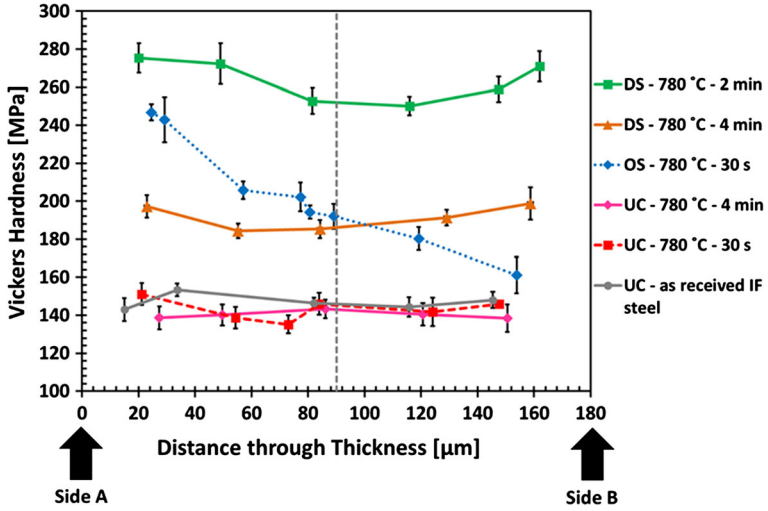

Fig. 3 Vickers microhardness through thickness for uncoated (UC) as-received IF steel, one-side-coated (OS) and double-side-coated (DS) IF steel after induction heating at different temperatures and times. Side A indicates one side of the sample and side B is the other side of the tensile coupon. The dashed line at the center of the graph indicates the thickness center. For the one-side-coated coupon (OS), side A is coated, while side B is without coating. Black error bars represent the standard deviation

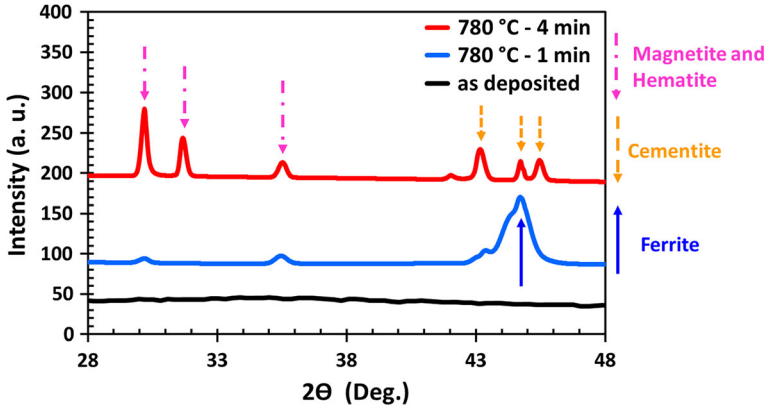

Fig. 4 Grazing angle X-ray diffraction of FeC films with 30 at.% of carbon after induction heating

a strong ferrite peak but most of the film is still amorphous, but after 4 min peaks corresponding to cementite are detected. The equation used to predict carbon diffusion through thickness is (Ref 20):

$$\frac{C(y,t)-C_s}{C_i-C_s}=\frac{4}{\pi}\sum_{n=0}^{+\infty}\left(\frac{(-1)^{n+1}}{2n+1}\right)*cos\left(\frac{2n+1}{2}\pi\frac{y}{L}\right)*exp\left(-\left(\frac{2n+1}{2}\frac{\pi}{L}\right)^2 Dt\right) \quad \text{(Eq 1)}$$

where $C(y,t)$ is the carbon concentration at position y (through thickness) and at time t, while C_s is the carbon concentration at the surface and C_i is the carbon concentration inside the IF steel. D is the diffusion coefficient of carbon in ferrite and L is the total length covered by diffusion. L is half the sample thickness for double-side-coated specimens or the full thickness for one-side-coated samples. Figure 5 shows the carbon profile for a double-side-coated coupon, and Fig. 6 shows the profile for a one-side-coated coupon.

These carbon profiles confirm that after 2 min of induction heating a small gradient is expected moving from the coated surface to the center, while in 4 min, the carbon profile is linear.

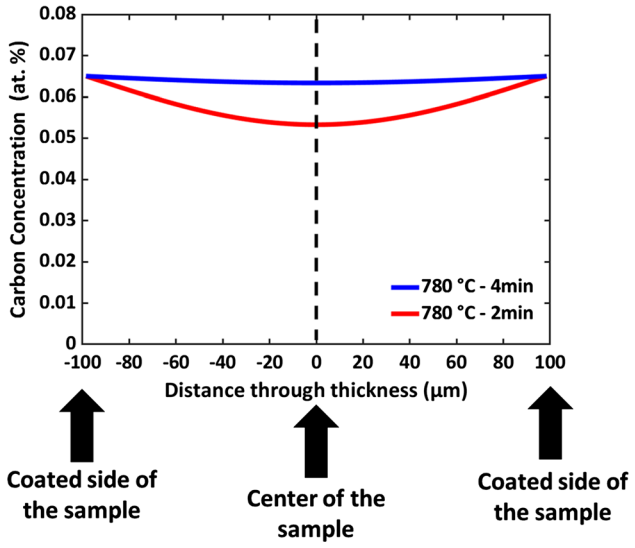

Fig. 5 Carbon distribution predicted theoretically using second Fick's diffusion law for heating at 780 °C for 2 and 4 min on a double-side-coated specimen

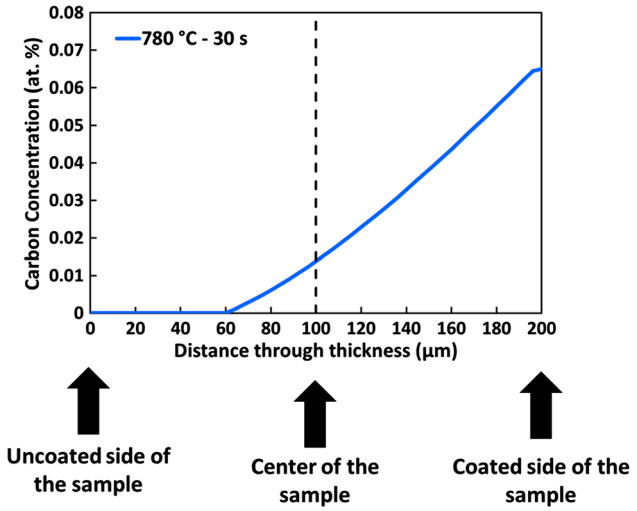

Fig. 6 Carbon distribution predicted theoretically using second Fick's diffusion law for heating at 780 °C for 30 s on a one-side-coated specimen

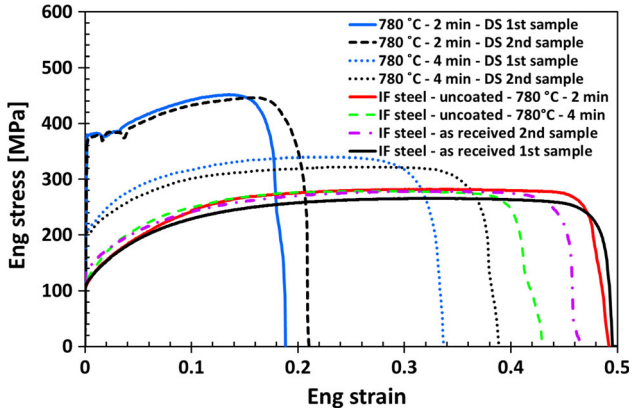

Fig. 7 Engineering stress–strain curves for coupons of IF steel-coated double sides (DS) with 500-nm-thick FeC film and induction heated for 2 and 4 min. Engineering stress–strain curves of uncoated and as-received IF steel and of uncoated but induction-heated specimens are included.

For an induction heating of 30 s on a sample coated only on one side, the carbon diffusion will not cover the whole thickness, and thus a large hardness gradient is obtained.

3.2 Tensile Tests

The engineering stress–strain curves obtained for double-sided coupons (DS) after induction heating and quenching are shown in Fig. 7. Two tensile curves for the as-received, uncoated IF steel are included as reference. The maximum increase in yield stress (374 ± 6 MPa) and ultimate tensile strength (448 ± 3.5 MPa) is obtained after 2 min of induction heating. After 4 min of induction heating, suppression of Lüdering is observed and the yield stress drops to 206 ±1.7 MPa with an ultimate tensile strength of 320 ± 12 MPa. Strain at fracture is 20 ± 1% for the sample double side coated and induction heated for 2 min, while strain at fracture is 36 ± 3% for induction heating performed 4 min in a double-side-coated sample. The maximization of strengthening after 2 min and the disappearance of Lüdering after 4 min of induction heating for coated samples are repeatable. Table 1 presents the average mechanical properties obtained from tensile tests for each condition with the calculated standard deviation. The deviations associated with yield strength and ultimate tensile strength for the induction-heated samples are in the range of ± 10 MPa, which is also the uncertainty range associated with the starting as-received IF steel. Engineering stress–strain curves of uncoated IF steel specimens induction heated at 780 °C for 2 min or 4 min are included in Fig. 7. The uncoated IF substrate shows no variation of yield stress and ultimate tensile strength after induction heating as shown in Table 1. The 2-4% standard deviation associated with the strain at fracture is due to the subsize geometry and thin thickness used for tensile specimens.

Figure 8 shows optical microscope images of the through thickness microstructure of uncoated specimens, where uniform grain size is preserved after induction heat treatment. No difference was found between the microstructure of the uncoated (as received) IF steel before and after induction heating; thus these specimens were not considered further for analyses. Moreover, from the mechanical properties shown in Fig. 3 and 7, the uncoated and induction-heated samples have no change in mechanical properties, suggesting that the IF substrate is stable and that improvement in mechanical properties for coated samples must be caused by carbon diffusion. The microstructure through thickness for double-side-coated samples was analyzed with optical microscopy after etching with a 4 vol.% Nital solution. Figure 9 shows a uniform microstructure through the whole thickness for both samples induction heated for 2 and 4 min. However, in Fig. 9(a) and (c) banded features running through the grains are visible, while these lines are absent for the sample induction heated for 4 min (Fig. 9b and d). To exclude the influence of sample preparation, the specimens were further polished and only slightly etched with 2 vol.% Nital and imaged with scanning electron microscope. Figure 10(a) shows the microstructure at half-thickness for the double-side-coated sample induction heated for 2 min, while Fig. 10(b) displays half-thickness for 4 min of induction heating. For both images, the grains close to the surface are on the left of the image, while the grains at the center (half-thickness) are on the right. Both microstructures are uniform moving from the surface towards the center of the specimens, but the banded features crossing the grains are visible in the 2 min induction-heated specimen (Fig. 10a), while they are absent after 4 min of induction heating (Fig. 10b). These bands are highlighted after etching where some zones of the grains are more etched than other zones.

3.3 Electron Microscope Analyses

Further analyses were performed on the specimens with the highest mechanical properties (i.e., double side coated) to understand the difference in mechanical behavior found for induction heating at 2 and 4 min. According to the iron-carbon phase diagram (Ref 28), when the sample is heated at 1100 °C its microstructure is made of austenite (γ-iron), but during quenching the microstructure transforms into ferrite (α-iron). However, depending on the amount of carbon present in the microstructure, some austenite can be preserved in the microstructure (residual austenite) after quenching at room temperature (Ref 29). Ferrite has a body centered cubic crystallographic structure, while austenite has a face-centered crystallographic structure, and thus electron backscattered

Table 1 Average yield stress, ultimate tensile strength (UTS) and strain at fracture with corresponding standard deviation obtained from tensile testing of uncoated and double-side coated induction-heated IF specimens

Specimen	Yield stress, MPa	UTS, MPa	Strain at fracture
As-received IF steel	116 ± 9	272 ± 8	0.48 ± 0.02
Uncoated IH 780 °C-2 min	113.6 ± 3.4	281 ± 2	0.48 ± 0.02
Uncoated IH 780 °C-4 min	117.4 ± 2.2	275 ± 4	0.46 ± 0.04
DS—IH 780 °C-2 min	374 ± 6	448 ± 3.5	0.2 ± 0.01
DS—IH 780 °C-4 min	206 ± 1.7	320 ± 12	0.36 ± 0.03

Mechanical properties of the uncoated and not induction heated IF steel are included.

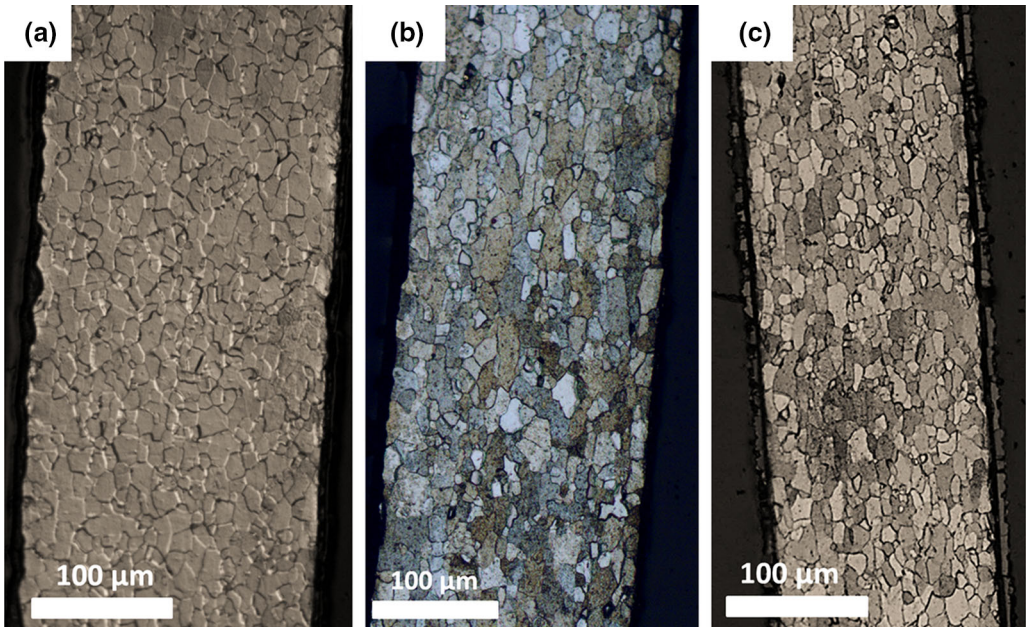

Fig. 8 Optical microscope images of thickness cross section for: uncoated and as-received IF (a), uncoated IF induction heated at 780 °C for 2 min (b), uncoated IF induction heated at 780 °C for 4 min (c)

diffraction (EBSD) can be employed to investigate the presence of different phases and to verify the presence of residual austenite. Data are shown in Appendix A. The two specimens did not show any remarkable difference in terms of phase maps (Fig. 17a and b in Appendix A) and band contrast maps (Fig. 18a and b in Appendix A) despite their strong difference in mechanical properties. Both samples have fully ferritic microstructure. Thus, transmission electron microscope (TEM) analyses were carried out. Figure 11 shows SEM and TEM images for microstructures in the middle of the double-sided coupons induction heated for 2 and 4 min. The specimen induction heated for 2 min shows non-uniform etching within the grains, revealing banded features going through the grains and across grain boundaries (Fig. 11a), while the specimen induction heated for 4 min had uniform etching throughout the grains (Fig. 11b). While the transformation of austenite into ferrite is known to be influenced by large magnetic fields (above 5 T) (Ref 30-33), the magnetic field intensities in the experiments presented here range between 7.5 and 10.5 mT which should not be sufficient to affect ferrite growth. TEM samples were extracted using focused ion beam (FIB) from an area inside the band and from an area surrounding the bands. From a first qualitative TEM imaging, one can observe that the bands found for the specimen induction heated for 2 min contain high densities of precipitates (Fig. 11c), while the surrounding material has lower density but larger precipitates (Fig. 11d). On the other hand, the specimen induction heated for 4 min shows a uniform microstructure with dislocations and some large precipitates (Fig. 11e).

Further TEM analyses were performed to understand the nature of these precipitates. These investigations confirmed that for both 2 min and 4 min of induction-heated specimens, the precipitates contain titanium and carbon and their diffraction pattern corresponds to TiC carbides. Figure 12(a) and (b) shows that in both microstructures nanosized precipitates and dislocations are found. A higher magnification image showing a region full of carbides is shown in Fig. 12(c). From diffraction pattern and energy-dispersive spectroscopy (EDS) analyses, the precipitates were identified as TiC (∼20 nm in diameter) as shown in Fig. 12(d) and (e).

Other spectra were obtained for both matrix and precipitates in the sample induction heated at 780 °C for 2 min (Fig. 13). Titanium is not detected in the matrix, but it is detected in the precipitates confirming the presence of TiC nanosized carbides. Other zones of the samples induction heated at 780 °C for 4 min were analyzed by acquiring EDS spectra (Fig. 14a). The spectre 1 from area 1 acquired inside the matrix shows strong peaks of iron but no carbon could be identified (Fig. 14). Here,

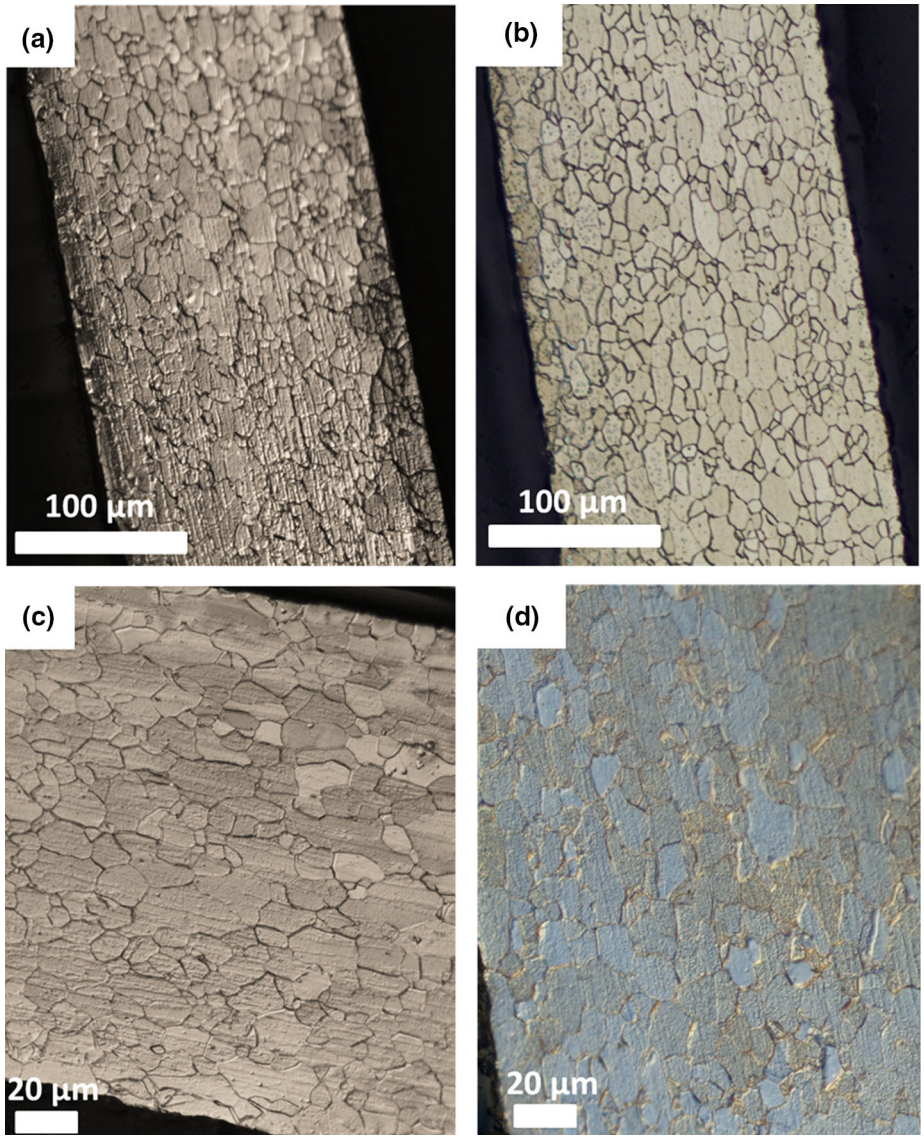

Fig. 9 Optical microscope images of thickness cross section for: double-side coated IF steel induction heated at 780 °C-2 min (a) and (c), double-side coated IF steel induction heated at 780 °C for 4 min (b) and (d)

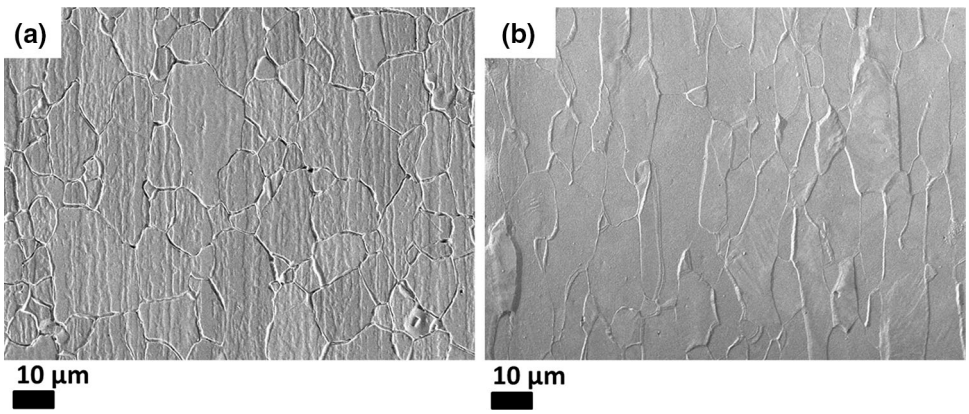

Fig. 10 Scanning Electron Microscope images of thickness cross section for: double-side coated IF steel induction heated at 780 °C-2 min (a) and double-side coated IF steel induction heated at 780 °C for 4 min (b)

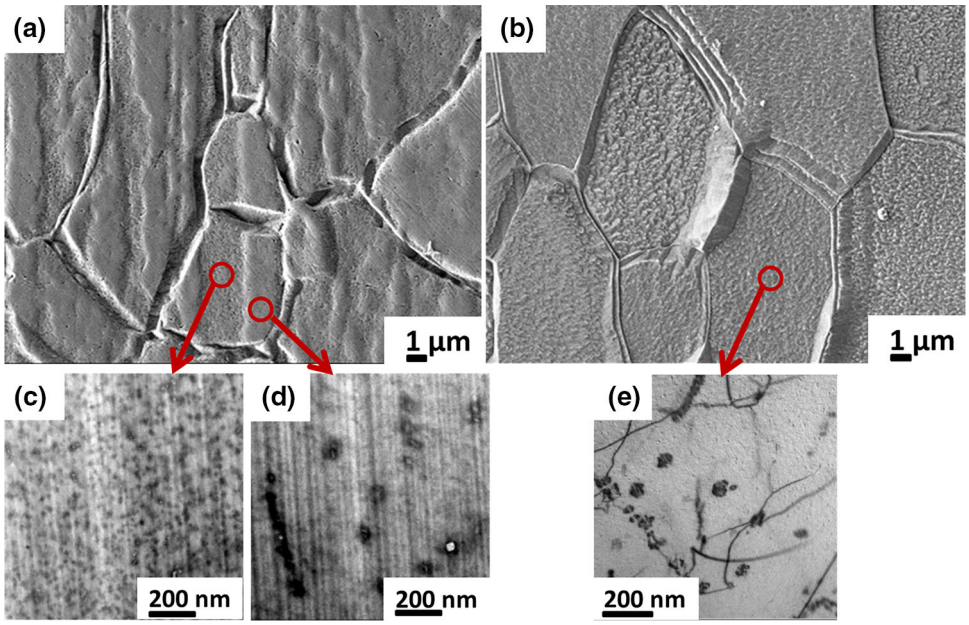

Fig. 11 SEM images of a specimen of IF steel double-side coated with 500 nm thick FeC film after induction heating at 780 °C-2 min (a) and at 780 °C-4 min (b). BF-STEM images obtained with TEM in a zone inside the bands (c) and surrounding the bands (d) for the specimen kept at 780 °C for 2 min. (e) BF-STEM image inside a grain for specimen kept at 780 °C for 4 min

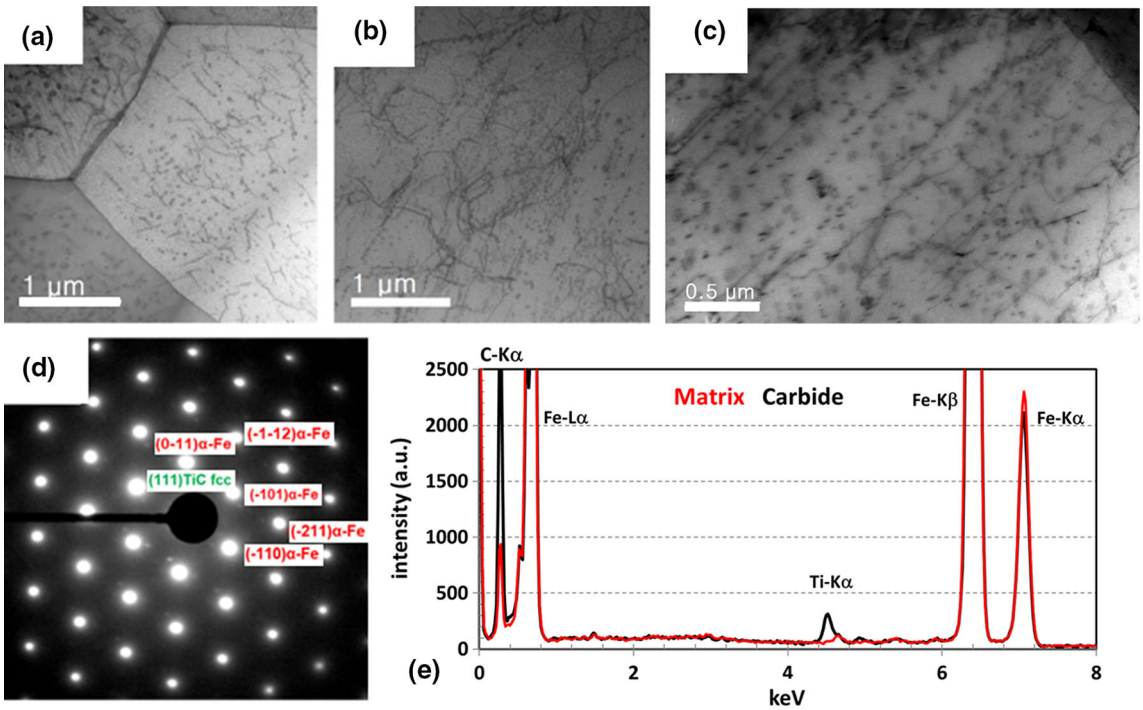

Fig. 12 BF-STEM image showing the distribution of TiC nanosize precipitates after 2 min (a) and 4 min (b) of induction heating at 780 °C. Example of regions where precipitates were indexed (c) and typical diffraction pattern taken in (111) α-Fe zone axis where (111) fcc TiC are indexed near (110) α-Fe and indicating a Kurdjumov-Sachs orientation relationship (d). EDS spectra recorded in the matrix and on a precipitate (e) where Ti and C are clearly detected (the strong Fe peak for the carbide curve is due to the surrounding matrix) for a specimen induction heated for 2 min

the intensity of the first peak is lower than the carbon peak identified in the matrix for specimen induction heated at 780 °C for 2 min and the intensity is not high enough to be identified as a relevant carbon concentration. Spectra 2, 3 and 4 acquired from precipitates (area 2, 3 and 4 in Fig. 14a) confirm higher carbon and titanium concentrations in precipitates than in the matrix (Fig. 14).

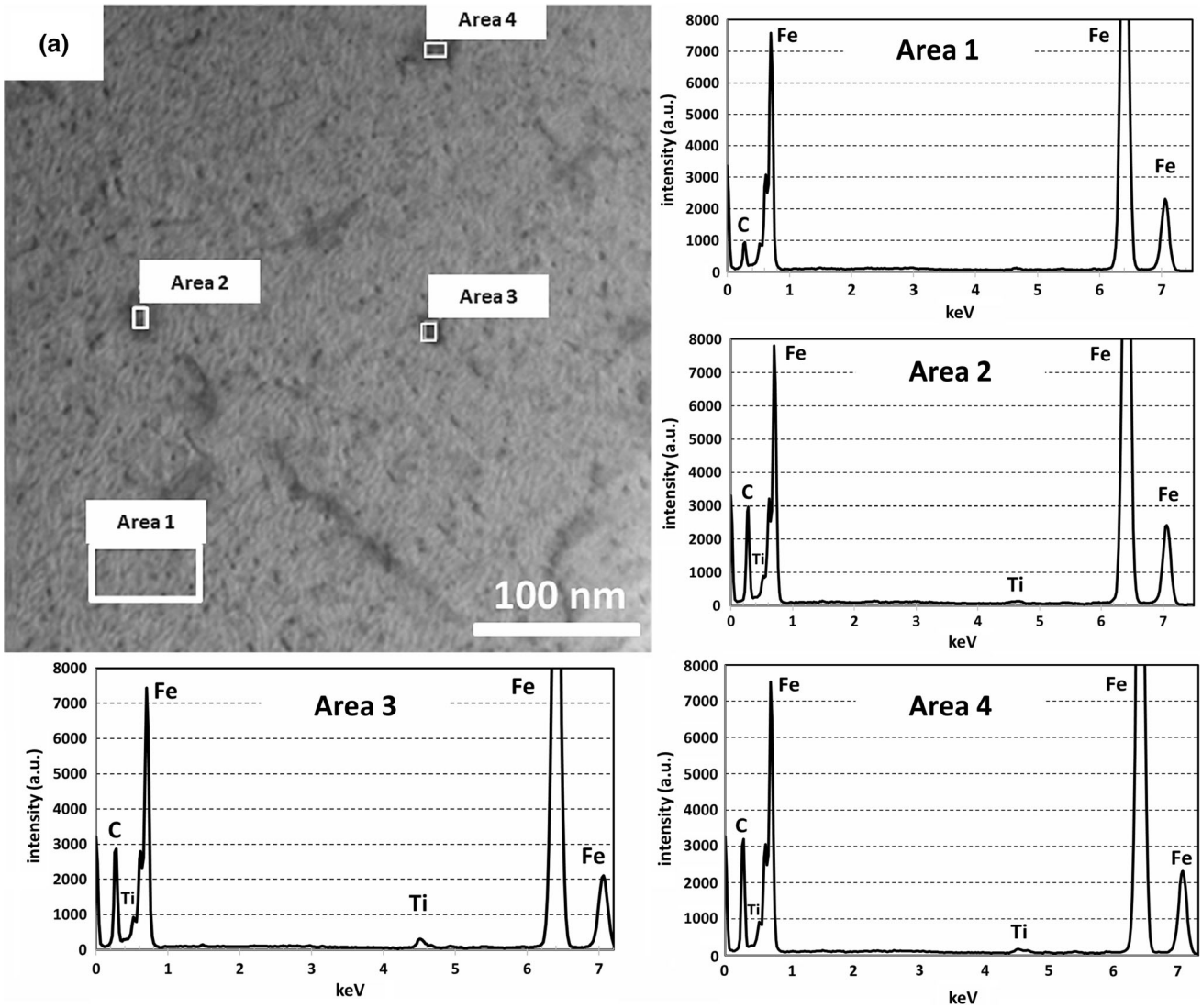

Fig. 13 BF-STEM image of the sample induction heated at 780 °C during 2 min showing in dark contrast lattice distortions created by dislocations and nanoscaled carbides (a). Locations of EDS spectra (1, 2, 3, 4) are indicated in the image. Area 1 is the reference taken in the matrix where Ti is below the detection limit. Area 2, 3 and 4 clearly exhibit the Ti-K peak, confirming the presence of nanoscaled TiC carbides.

4. Discussion

The presence of nanoscale precipitates is known to enhance the strength of steels. Xu et al. (Ref 34) found a yield stress of 420 MPa for a steel containing 0.034 wt.% of titanium. This strength was attributed to the precipitation of nanoscale TiC that cause strengthening by impeding dislocation motion.

In the work of Hong et al. (Ref 35), the precipitation of TiC carbides in a ferrite/pearlite microstructure resulted in a yield stress of 372 MPa, which is very close to the yield stress obtained in the present work (374 MPa). In their work, Hong et al. (Ref 35) showed that TiC carbides are dissolved at 1100 °C and are precipitated during cooling in the temperatures range 800-920 °C. Wang et al. (Ref 36) found the precipitation of TiC carbides periodically at the austenite/ferrite interphase following the movement of the interface and along the hot rolling direction of the steel. Moreover, Kobayashi et al. (Ref 37) have shown that TiC precipitates are formed more easily in pre-deformed ferritic steel compared to undeformed steel due to the higher density of dislocations. Samples induction heated for 2 min show Lüdering which is known to be caused by the interaction of small atoms (i.e., carbon) present in solid solution with dislocations. This suggests that after 2 min not all the carbon is precipitated but part of it must still be in solid solution pinning dislocations.

The suppression of Lüdering after 4 min of induction heating is most likely due to a decrease or absence of carbon in solid solution and thus full stabilization of carbon. This complete precipitation of carbon could occur through TiC precipitation or coarsening. Coarsening of TiC and the consequent decrease in hardness were reported by Wang et al. (Ref 36) and by Dunlop et al. (Ref 38). Another contribution to carbon stabilization in IF steels is due to TiS precipitates that can transform into $Ti_4C_2S_2$ by removing carbon from dislocations at temperatures above 700 °C (Ref 39).

In all induction-heated samples, precipitates containing titanium and sulfur as well as precipitates containing titanium, carbon and sulfur were found (respectively, Fig. 15 and 16). Thus, TiS precipitates are expected to play a role in the precipitation of carbon when the isothermal holding time at temperatures equal or higher than 700 °C is increased.

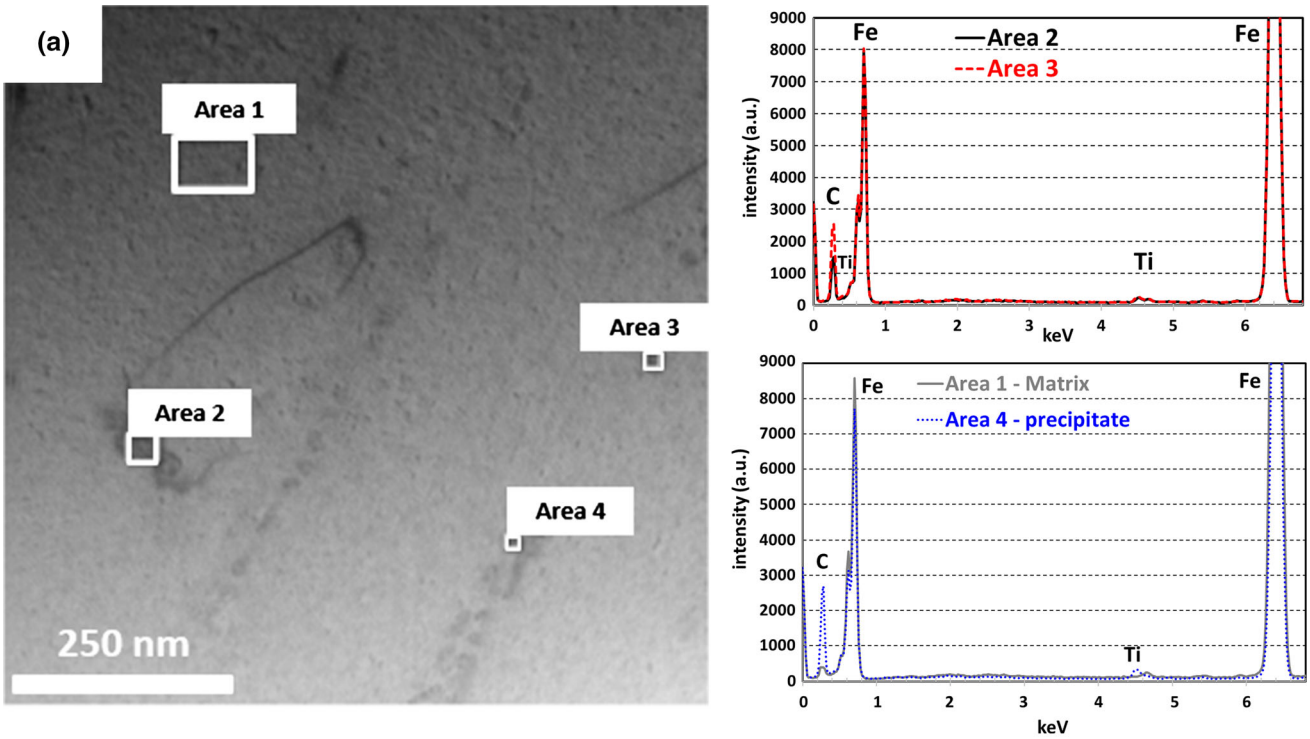

Fig. 14 BF-STEM image of the sample induction heated at 780 °C for 4 min showing in dark contrast lattice distortions created by dislocations and nanoscaled carbides (a). Locations of EDS spectra (1, 2, 3 and 4) are indicated in the image. Area 1 is obtained from the matrix, while Area 2, 3 and 4 show measurements obtained from nanoscaled precipitates

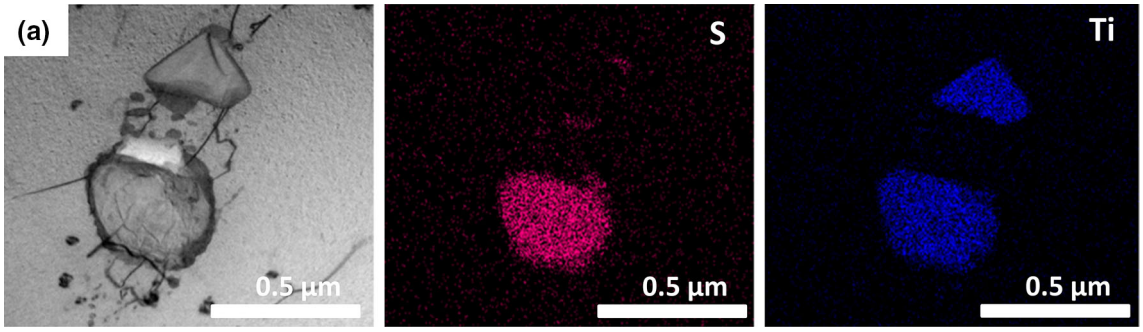

Fig. 15 BF-STEM image from a micronsized precipitate found in induction-heated IF double-side-coated steel samples (a). EDS composition maps show that it contains titanium and sulfur

Referring to the work of Hong et al. (Ref 35), the yield strength for specimens induction heated for 2 and 4 min was predicted calculating the contribution from strengthening due to nanoprecipitates, grain boundaries, carbon in solid solution and dislocations. The strengthening caused by nanoprecipitates was evaluated through the Ashby–Orowan equation (Ref 35):

$$\sigma_{NP} = \left(\frac{0.13 \cdot G \cdot b}{\lambda}\right) \cdot \ln\left(\frac{r}{b}\right) \quad \text{(Eq 2)}$$

where G is the iron shear modulus (82 GPa), b is the iron Burgers vector (0.286 nm), λ is the spacing between precipitates and r the precipitate radius (in the present work ~10 nm). The spacing between precipitates can be calculated with:

$$\lambda = d_p \left[\frac{1}{(0.5.V_p)^{1/3}} - 1\right] \quad \text{(Eq 3)}$$

where d_p is the average particle diameter and V_p is the volume fraction of nanoparticles (Ref 35).

The volume fraction of precipitates (V_p) in Eq 3 is calculated by multiplying the density of precipitates extracted from TEM bright-field images by the mean volume of a single precipitate assuming a spherical shape and an average diameter of 20 nm. Thus, the volume of a single precipitate will be 4.18×10^{-24} m^3. The density of precipitates from TEM images is calculated by using the multipoint tool in Image J (Ref 40) after enhancing the contrast of bright-field TEM images. The number of precipitates is then divided by the volume of the TEM sample. This method for calculating particles density can be applied to the TEM images taken at each induction heating condition. For 2 min of induction heating, the density of precipitates was estimated to be 3.33×10^{20} m^{-3}, while it was estimated to be 3.67×10^{20} m^{-3} after 4 min of induction heating. Multiplying

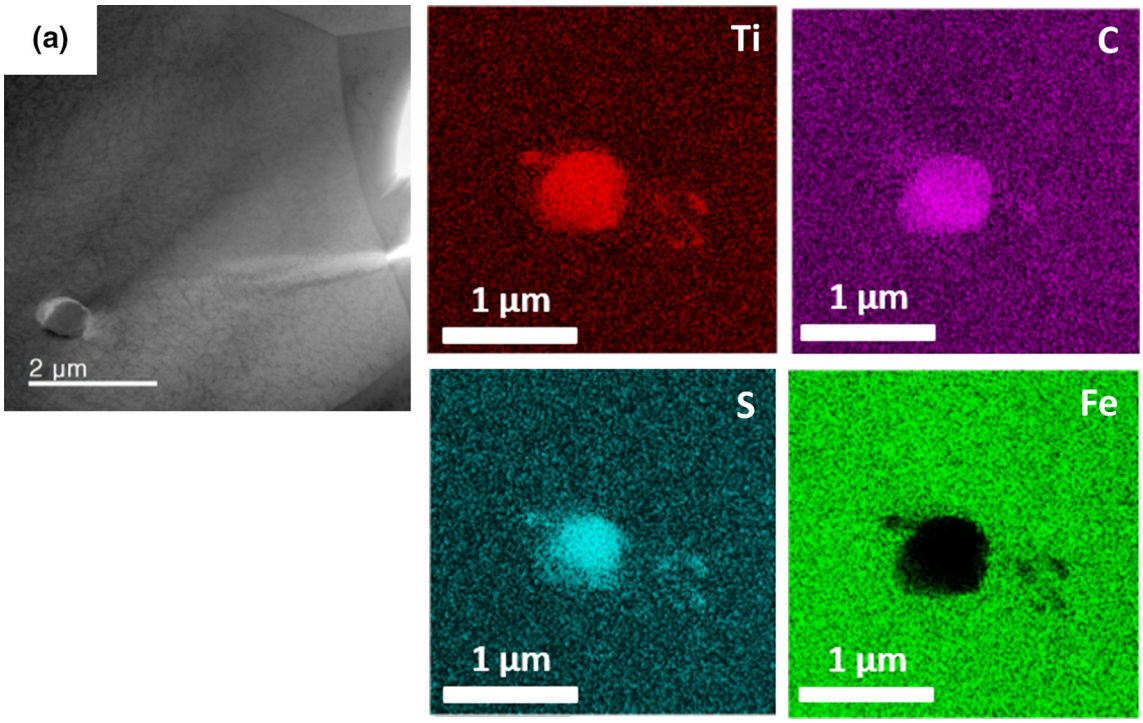

Fig. 16 BF-STEM image obtained from a coarse precipitate found in induction-heated IF double-side-coated steel samples (a). According to EDS composition maps, this precipitate contains titanium, sulfur and carbon

this density of precipitates by the volume of a single precipitate will give the volume fraction (V_p) to be used in Eq 3. The fraction of precipitates was calculated to be 1.39×10^{-3} for 2 min and 1.54×10^{-3} for 4 min of induction heating. The strengthening due to grain boundaries (σ_{GB}) is calculated with the Hall–Petch equation as $K \cdot d^{-1/2}$ where K is the Hall–Petch coefficient and d is the average grain size (Ref 41). The Hall–Petch coefficient (K) depends on the amount of carbon segregation present in the steel (Ref 41). The strengthening caused by carbon in solid solution (σ_{SS}) is calculated as $Mm(X_C)^{1/2}$, where M is the Taylor factor (here 2.5), m is equal to 0.051 times the iron shear modulus (82 GPa) and X_C represents the atomic fraction of carbon in solid solution at dislocations (Ref 20, 42). Finally, the strengthening due to dislocations (σ_{DIS}) can be calculated as $(\alpha Gb)\rho^{1/2}$, where α is the dislocation parameter and it is set equal to 0.5, G and b are the shear modulus of iron (82 GPa) and the Burgers vector (0.286 nm), respectively, ρ is the dislocation density (Ref 35). Dislocation density was calculated using the relation reported by Hong et al. (Ref 35) and obtained by Zhang et al. (Ref 43):

$$\rho = \left[\frac{12 \cdot \Delta\delta \cdot \Delta T \cdot V_p}{b \cdot d_p(1 - V_p)}\right] \quad \text{(Eq 4)}$$

where $\Delta\delta$ is the difference in the coefficient of thermal expansion (CTE) between the reinforcement particle (TiC) and the matrix (ferrite) (i.e., 5×10^{-6} °C^{-1}, by considering a CTE of 12×10^{-6} °C^{-1} for pure iron and a 7.0-7.2 $\times 10^{-6}$ °C^{-1} for titanium carbide (Ref 44), ΔT is the difference between test (i.e., 25 °C) and heat treatment temperatures (i.e., 780 °C).

From Eq 4, the calculated dislocation density is 1.11×10^7 mm^{-2} for the specimen induction heated 2 min and 1.22×10^7 mm^{-2} after 4 min, which will result in a dislocation strengthening (σ_{DIS}) of 39 MPa and of 41 MPa for the 2-min and 4-min specimens, respectively.

All these strengthening contributions have been calculated for both specimens (2 min and 4 min) and are shown in Table 2. The yield stress of the uncoated as-received IF steel is evaluated considering that its friction stress is 50 MPa (Ref 41, 45) and the grain boundary strengthening (σ_{GB}) of the IF steel substrate is 50 MPa (considering a Hall–Petch coefficient of 180 MPa·μm$^{1/2}$ and a measured average grain size for the as-received IF steel substrate of 13 μm). Thus, the yield strength predicted for the starting IF steel is 100 MPa, which is in good agreement with the yield stress obtained experimentally of 116 ± 9 MPa (Table 2).

After 2 min, the amount of carbon diffused into steel is at most 0.0645 at.% because of film crystallization and part of this carbon interacts with the 0.050 at.% of titanium initially present in the steel to form TiC. Thus, the carbon available to strengthen grain boundaries and dislocations is 0.0145 at.%. This amount of carbon can be used to calculate the solid solution strengthening (σ_{SS}) by using a Taylor factor of 2.5, an m of 0.051 and the iron shear modulus of 82 GPa, which give 126 MPa of solid solution strengthening (Table 2). Another contribution to strengthening comes from grain boundaries (σ_{GB}) calculated using the Hall–Petch equation. For the specimen induction heated for 2 min, the Hall–Petch coefficient was obtained from the work of Takaki (Ref 45) considering that 0.0145 at.% of carbon (corresponding to 31 weight ppm) is available inside 2-min induction-heated samples and that would correspond to a Hall–Petch coefficient of 400 MPa·μm$^{1/2}$. Moreover, the measured average grain size is 15 μm resulting in a grain boundary strengthening (σ_{GB}) of 103 MPa (Table 2).

Table 2 Comparison between theoretically calculated strengthening with results obtained experimentally: σ_{NP} indicates strengthening due to nanoprecipitates, σ_{GB} is the strengthening due to grain boundaries, σ_{SS} is the contribution of carbon in solid solution, σ_{DIS} is the contribution to strengthening coming from dislocations

	Friction stress IF steel σ_0, MPa	TiC Particle density, m^{-3}	Dislocation density, mm^{-2}	σ_{NP}, MPa	σ_{GB}, MPa	σ_{SS}, MPa	σ_{DIS}, MPa	$\sigma_{YS\ Theor.}$, MPa	$\sigma_{YS\ Exper.}$, MPa
Unc.	50	…	…	…	50	…	…	100	116 ± 9
2 min	50	3.33×10^{20}	1.11×10^{7}	53	103	126	39	371	374 ± 6
4 min	50	3.67×10^{20}	1.22×10^{7}	55	46.5	0	41	192.5	206 ± 1.7

The theoretical total strengthening σ_{YST} was calculated by summation of all contributions:

$$\sigma_{YST} = \sigma_0 + \sigma_{NP} + \sigma_{GB} + \sigma_{SS} + \sigma_{DIS} \quad \text{(Eq 5)}$$

where σ_{YST} is the yield stress, σ_0 is the friction stress, σ_{NP} is the strength caused by nanoprecipitates, σ_{GB} is the strengthening due to grain boundary, σ_{SS} is the contribution due to carbon in solid solution (i.e., at dislocations) and σ_{DIS} is the strengthening due to dislocations.

For the specimen induction heated for 2 min, the yield stress theoretically predicted of 371 MPa is in good agreement with the yield stress measured experimentally of 374 ± 6 MPa.

When induction heating is prolonged for 4 min at 780 °C, Lüdering disappears and the yield stress is lowered. It is believed that all the carbon has precipitated and solid solution strengthening does not contribute anymore. Even if it is difficult to measure precisely carbon content with EDS, a relative comparison among the samples can be done. From TEM EDS analyses, the matrix of sample induction heated for 4 min did not show a carbon peak, while the specimen induction heated for 2 min had a carbon peak with an intensity strong enough to conclude that some carbon is present in the ferrite matrix. However, no significant decrease in the density of TiC carbides was found from TEM analyses (i.e., sample induction heated for 4 min has higher particle density than the sample annealed for 2 min), and thus it is believed that the carbon remaining in solid solution takes part in the transformation of TiS particles into $Ti_4C_2S_2$ as discussed in the literature for IF and ultra-low-carbon steels (Ref 20, 46) or to coarsening of some TiC precipitates. TiS precipitates containing carbon were found during TEM analyses on our annealed specimens. Thus, the contribution from solid solution strengthening can be removed because all carbon has precipitated in the 4 min of induction-heated specimen. For this sample, the grain boundary strengthening is estimated to be 46.5 MPa (Table 2) when the same Hall–Petch coefficient (180 MPa·$\mu m^{1/2}$) of an uncoated and as-received IF steel (i.e., all carbon has precipitated) and a measured average grain size of 15 μm are considered. By summing linearly all the contributions for the 4 min of induction-heated specimen, the expected yield stress is 192.5 MPa, in good agreement with the experimental value of 206 ± 1.7 MPa (Table 2).

Considering the hardness values in Fig. 3, the highest hardness is found in the sample induction heated at 780 °C for 2 min because there is a strengthening contribution coming both from precipitates and carbon in solid solution. This means that when the material is plastically deformed through Vickers microhardness, dislocations will interact both with carbides and carbon in solid solution. The highest hardness is in agreement with the highest yield stress and ultimate tensile strength found in the tensile tests. For the sample annealed at 780 °C for 4 min, the hardness is lower than the hardness of the 2 min sample because all the carbon is precipitated and no carbon is left in solid solution.

5. Conclusions

In conclusion, amorphous FeC films can be used as carbon reservoirs to diffuse carbon not only during isothermal annealing but also during induction heat treatments. The advantage of induction heating is the fast heating rate that allows reaching rapidly the required temperature promoting carbon diffusion before complete crystallization of the FeC film. This type of process is promising to obtain high-strength IF steels with short annealing times (2 min) and carbon graded steels in just 30 s. For 2 min of induction heating, the maximum yield strength is 374 ± 6 MPa. This high strength is caused by carbon present both in solid solution and as TiC precipitates added to further strengthening contributions from grain boundaries and dislocations. Induction heating for 2 min gives a strain at fracture of 20%. This strain at fracture is 30% lower than non-strengthened (as received) IF steel but it is comparable to the strain at fracture of commercial TRIP steels. It can be argued that such strengthened IF steel would not be formable through conventional deep-drawing techniques; however, high strain rate forming techniques such as electro-hydraulic forming or explosion forming are starting to be used for industrial components (Ref 47) because they can improve formability (Ref 48). An increase of annealing time from 2 to 4 min causes an increase in strength of 100 MPa compared to the as-received IF steel, but carbon atoms are believed to be fully stabilized causing Lüdering suppression. The full precipitation of carbon cancels out the contribution to strengthening from solid solution. Thus, the 4 min of induction-heated specimen will only have contribution to strengthening from TiC precipitates, grain boundaries and dislocations. The strengthening process presented in this paper could be very relevant to steel companies because high-strength IF steel could be obtained in few minutes of heat treatment resulting in an increase of yield stress higher than the increase obtained currently in bake-hardenable ultra-low-carbon steels. Moreover, the formation of nanoprecipitates in a ferrite matrix is of great interest to open new processing routes to obtain a good compromise between strength and ductility (Ref 49).

Another advantage of the processing method presented in this paper is the versatility of FeC films and induction heating. The amount of carbon in the film could be increased above 30 at. %, to allow more carbon diffusion into the IF substrate and promote the formation of non-equilibrium structures such as

martensite or bainite upon quenching. The authors presented a qualitative discussion of the advantages of FeC films for steel companies in terms of performance, marketability and sustainability and the idea has gathered high interest in the steel community (Ref 50).

Acknowledgments

The support of Dr. Ben Lawrence from University of British Columbia for the physical vapor deposition (PVD) coating is acknowledged.

Author's Contribution

EC contributed to conceptualization, methodology, validation, formal analysis, investigation, writing original draft, writing–review and editing. XS contributed to methodology, validation, formal analysis, investigation, resources, writing–review and editing, funding acquisition. CPS contributed to writing–review and editing, supervision, project administration, funding acquisition. AW contributed to validation, investigation, resources, writing–review and editing, supervision, funding acquisition.

Funding

This work was performed with the funding of the Natural Sciences and Engineering Research Council of Canada (NSERC) and Agence Nationale de la Recherche (ANR) through the GRaCoS project (ANR-09-BLAN-0412). The raw IF steel was supplied by ArcelorMittal.

Conflict of interest

The authors report no declarations of interest.

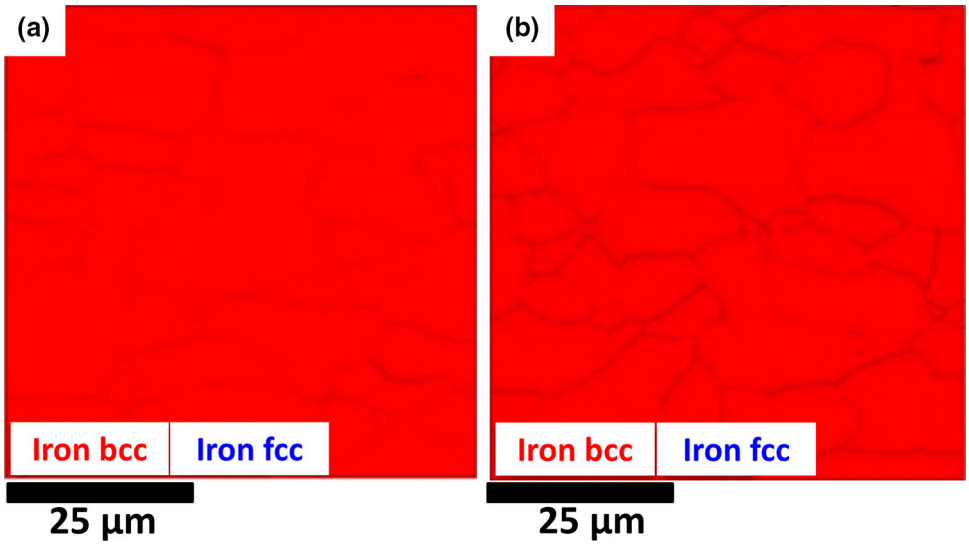

Fig. 17 Phase maps obtained from EBSD for specimens induction heated at 780 °C for 2 min (a) and 4 min (b)

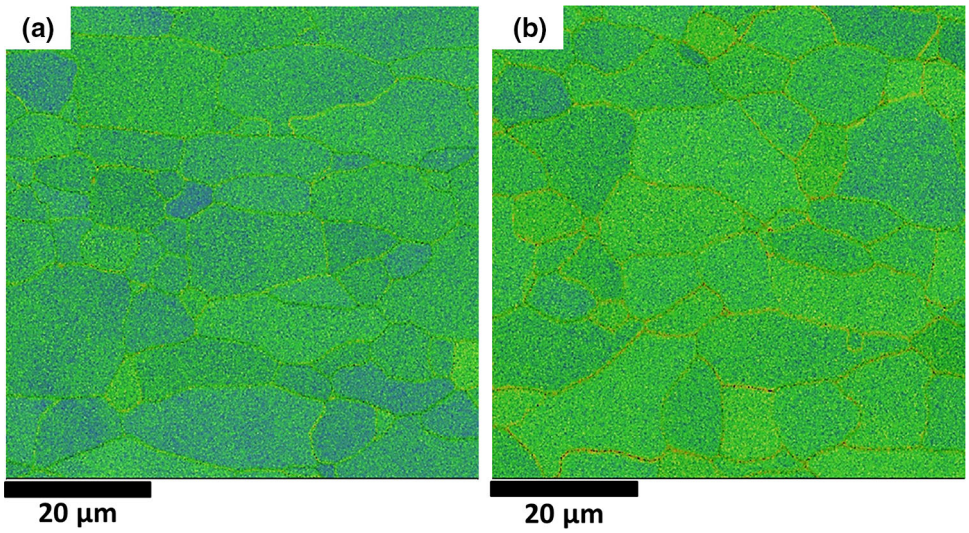

Fig. 18 Local misorientation and band contrast maps obtained from EBSD for specimens induction heated at 780 °C for 2 min (a) and 4 min (b)

Appendix A

EBSD was performed for samples induction heated for 2 min and 4 min to obtain phase maps of the microstructure. Specimens were polished down to mirror finish with OPS silica solution. More precisely, OPS polishing was performed for a total of 5 min, and in between this time the surface was slightly etched with 4 vol.% Nital to ensure no influence from mechanical polishing. For both samples, EBSD was performed in an area of 65 × 65 μm using a step of 0.1 μm. Figure 17(a) and (b) show phase maps for both samples, while Fig. 18(a) and (b) show local misorientation plus band contrast maps. 18

References

1. Y. Weng, H. Dong, Gan Y, *Advanced Steels: The Recent Scenario in Steel Science and Technology*, Springer-Verlag Berlin Heidelberg—Metallurgical Industry Press, (2011)
2. L.J. Baker, S.R. Daniel, J.D. Parker, Metallurgy and Processing of Ultralow Carbon Bake Hardening Steels, *Mater. Sci. Technol.*, 2002, **18**(4), p 355–368.
3. Y. Tanaka, T. Urabe, Y. Nagataki, A New Type of High Strength Steel for Exposed Panels: High-Strength Steel with Excellent Formability, Superior Surface Precision after Press Forming, and Uniform Surface Appearance, *JFE Tech. Rep.*, 2004, **4**(4), p 17–24.
4. A. Itami, K. Ushioda, N. Kimura, H. Asano, Y. Kimura, K. Koyama, Development of New Formable Cold-Rolled Sheet Steels for Automobile Body Panels, *Nippon Steel Technical Report*, (1995), pp. 26–32
5. ArcelorMittal, "High Strength IF Steels," https://automotive.arcelormittal.com/products/flat/HYTSS/IF, n.d
6. D. Krizan, B.C. De Cooman, Mechanical Properties of TRIP Steel Microalloyed with Ti, *Metall. Mater. Trans. A Phys. Metall. Mater. Sci.*, 2014, **45**(8), p 3481–3492.
7. R. Rana, W. Bleck, S.B. Singh, O.N. Mohanty, Development of High Strength Interstitial Free Steel by Copper Precipitation Hardening, *Mater. Lett.*, 2007, **61**(14–15), p 2919–2922.
8. Y.Z. Shen, K.H. Oh, D.N. Lee, Nitrogen Strengthening of Interstitial-Free Steel by Nitriding in Potassium Nitrate Salt Bath, *Mater. Sci. Eng. A*, 2006, **434**(1–2), p 314–318.
9. T. Gladman, *The Physical Metallurgy of Microalloyed Steels*, Maney for the Institute of Materials, (2002)
10. D.S. Mersagh, M. Sabzi, Deposition of Ceramic Nanocomposite Coatings by Electroplating Process: A Review of Layer-Deposition Mechanisms and Effective Parameters on the Formation of the Coating, *Ceram. Int.*, 2019, **45**(17), p 21835–21842.
11. M. Sabzi, S. Mersagh Dezfuli, Deposition of Al_2O_3 Ceramic Film on Copper-Based Heterostructured Coatings by Aluminizing Process: Study of the Electrochemical Responses and Corrosion Mechanism of the Coating, *Int. J. Appl. Ceram. Technol.*, 2019, **16**(1), p 195–210.
12. S.H. Mousavi Anijdan, M. Sabzi, M. Asadian and H.R. Jafarian, Effect of Sub-Layer Temperature during HFCVD Process on Morphology and Corrosion Behavior of Tungsten Carbide Coating, *Int. J. Appl. Ceram. Technol.*, 2019, **16**(1), p 243–253.
13. M. Sabzi, S.M. Far and S.M. Dezfuli, Characterization of bioactivity Behavior and Corrosion Responses of Hydroxyapatite-ZnO Nanostructured Coating Deposited on NiTi Shape memory Alloy, *Ceram. Int.*, 2018, **44**(17), p 21395–21405. https://doi.org/10.1016/j.ceramint.2018.08.197
14. S. Mersagh Dezfuli and M. Sabzi, Deposition of Self-Healing Thin Films by the Sol-Gel Method: A Review of Layer-Deposition Mechanisms and Activation of Self-Healing Mechanisms, *Appl. Phys. A Mater. Sci. Process*, 2019, **125**(8), p 1–8. https://doi.org/10.1007/s00339-019-2854-8
15. S. Sabooni, M. Ahmadi, E. Galinmoghaddam, R.J. Westerwaal, C. Boelsma, E. Zoestbergen, G.M. Song and Y.T. Pei, Fundamentals of the Adhesion of Physical Vapor Deposited ZnMg-Zn Bilayer Coatings to Steel Substrates, *Mater. Des.*, 2020, **190**, p 108560. https://doi.org/10.1016/j.matdes.2020.108560
16. B. Navinšek, P. Panjan and I. Milošev, PVD Coatings as an Environmentally Clean Alternative to Electroplating and Electroless Processes, *Surf. Coat. Technol.*, 1999, **116–119**, p 476–487.
17 . V. Rudnev, D. Loveless, and R.L. Cook, *Handbook of Induction Heating*, CRC Press, Taylor & Francis Group, (2017)
18. Y. Koizumi, T. Otsuka, Y. Minamino, T. Takayama, M. Ueyama, T. Daio and S. Hata, Microstructures Developed by Super-Rapid Induction Heating-and-Quenching (SRIHQ) of Fe-1.4%Cr-1%C Pearlitic Steel, *Mater. Sci. Eng. A*, 2013, **577**, p 29–35. https://doi.org/10.1016/j.msea.2013.04.024
19. C.P. Scott, C. Sinclair and A. Weck, Amorphous Fe1-XCx Coatings as Carbon Reservoirs for Diffusion Strengthening of Steel Sheets, *Scr. Mater.*, 2011, **65**(9), p 763–766. https://doi.org/10.1016/j.scriptamat.2011.07.023
20. E. Cantergiani, A. Fillon, B. Lawrence, X. Sauvage, M. Perez, C.P. Scott and A. Weck, Tailoring the Mechanical Properties of Steel Sheets Using FeC Films and Diffusion Annealing, *Mater. Sci. Eng. A*, 2016, **657**, p 291–298.
21. A. Fillon, X. Sauvage, B. Lawrence, C. Sinclair, M. Perez, A. Weck, E. Cantergiani, T. Epicier and C.P. Scott, On the Direct Nucleation and Growth of Ferrite and Cementite without Austenite, *Scr. Mater.*, 2015, **95**(1), p 35–38.
22. D. Wohlfahrt and R. Jürgens, Information Technology and Electrical Engineering: Devices and Systems, Materials and Technologies for the Future, In: *51st Internationales Wissenschaftliches Kolloquium*, (Technische Universität Ilmenau), (2006)
23. L. Weiner, P. Chiotti, and H.A. Wilhelm, Temperature Dependence of Electrical Resistivity of Metals. J. Phys. Soc. Japan (1952)
24. N. Abe and T. Suzuki, Thermoelectric Power Versus Electrical Conductivity Plot for Quench-Ageing of Low-Carbon Aluminium-Killed Steel, *Trans. Iron Steel Inst Japan*, 1980, **20**(10), p 690–695.
25. E. Bauer-Grosse, Thermal Stability and Crystallization Studies of Amorphous TM-C Films, *Thin Solid Films*, 2004, **447–448**(03), p 311–315.
26. E. Bauer-Grosse and G. LeCaer, Crystallisation of Amorphous Fe1-XCx Alloys ($0.30 < x < 0.32$) and Chemical Twinning, *J. Phys. F Met. Phys.*, 1986, **16**, p 399–406.
27. B. Lawrence, The Production and Crystallization of Amorphous Fe-C Alloys, (2017)https://doi.org/10.14288/1.0355248
28. H. Okamoto, The C-Fe (Carbon-Iron) System, *J. Phase Equilibria*, 1992, **13**(5), p 543–565.
29. O.D. Sherby, J. Wadsworth, D.R. Lesuer and C.K. Syn, Revisiting the Structure of Martensite in Iron-Carbon Steels, *Mater. Trans.*, 2008, **49**(9), p 2016–2027.
30. Y. Zhang, C. He, X. Zhao, L. Zuo, C. Esling and J. He, New Microstructural Features Occurring during Transformation from Austenite to Ferrite under the Kinetic Influence of Magnetic Field in a Medium Carbon Steel, *J. Magn. Magn. Mater.*, 2004, **284**(1–3), p 287–293.
31. M. Shimotomai, K. Maruta, K. Mine and M. Matsui, Formation of Aligned Two-Phase Microstructures by Applying a Magnetic Field during the Austenite to Ferrite Transformation in Steels, *Acta Mater.*, 2003, **51**(10), p 2921–2932.
32. M. Shimotomai, K. Maruta, Aligned Two-Phase Structures in Fe-C Alloys, *Scripta Mater.*, 2000, **42**(5), p 499–503.
33. T. Garcin, *Thermodynamics and Kinetic Effects of Static Magnetic Field on Phase Transformation in Low Alloy Steels*, Université Joseph-Fourier-Grenoble I, (2009), https://tel.archives-ouvertes.fr/tel-00519996
34. G. Xu, X. Gan, G. Ma, F. Luo, H. Zou, The Development of Ti-Alloyed High Strength Microalloy Steel, *Mater. Des.*, 2010, **31**(6), p 2891–2896. https://doi.org/10.1016/j.matdes.2009.12.032
35. S.M. Hong, E.K. Park, J.J. Park, M.K. Lee, J. Gu Lee, Effect of Nano-Sized TiC Particle Addition on Microstructure and Mechanical Properties of SA-106B Carbon Steel, *Mater. Sci. Eng. A*, 2015, **643**, p 37–46. https://doi.org/10.1016/j.msea.2015.07.026
36. T.P. Wang, F.H. Kao, S.H. Wang, J.R. Yang, C.Y. Huang, H.R. Chen, Isothermal Treatment Influence on Nanometer-Size Carbide Precipitation of Titanium-Bearing Low Carbon Steel, *Mater. Lett.*, 2011, **65**(2), p 396–399. https://doi.org/10.1016/j.matlet.2010.10.022
37. Y. Kobayashi, J. Takahashi, K. Kawakami, Effects of Dislocations on the Early Stage of TiC Precipitation Kinetics in Ferritic Steel: A Comparative Study with and without a Pre-Deformation, *Acta Mater.*, 2019, **176**, p 145–154. https://doi.org/10.1016/j.actamat.2019.06.055

38. G. Dunlop, R. Honeycombe, Ageing Characteristics of VC, TiC, and (V, Ti)C Dispersions in Ferrite, *Met. Sci.*, 1978, **12**(8), p 367–371. https://doi.org/10.1179/msc.1978.12.8.367
39. M. Hua, C.I. Garcia, A.J. Deardo, Precipitation Behavior in Ultra-Low-Carbon Steels Containing Titanium and Niobium, *Trans. A Phys. Metall. Mater. Sci.*, 1997, **28**(9), p 1769–1780.
40. W.S. Rasband, "Image J," n.d., http://imagej.nih.gov/ij/
41. S. Takaki, D. Akama, N. Nakada, T. Tsuchiyama, Effect of Grain Boundary Segregation of Interstitial Elements on Hall-Petch Coefficient in Steels, *Mater. Trans. - Spec. Issue Strength Fine Grained Mater. - 60 Years Hall–Petch*, 2013, **55**(1), p 28–34.
42. M.J. Roberts, W.S. Owen, *Physical Properties of Martensite and Bainite*, Special Report no.93, The Iron and Steel Institute, 1965, pp. 171–178
43. Z. Zhang, D.L. Chen, Consideration of Orowan Strengthening Effect in Particulate-Reinforced Metal Matrix Nanocomposites: A Model for Predicting Their Yield Strength, *Scr. Mater.*, 2006, **54**(7), p 1321–1326.
44. R.O. Elliott, C.P. Kempter, Thermal Expansion of Some Transition Metal Carbides, *J. Phys. Chem.*, 1958, **62**(5), p 630–631.
45. S. Takaki, Review on the Hall-Petch Relation in Ferritic Steel, *Mater. Sci. Forum*, 2010, **654–656**, p 11–16.
46. S. Carabajar, J. Merlin, V. Massardier, S. Chabanet, Precipitation Evolution during the Annealing of an Interstitial-Free Steel, *Mater. Sci. Eng. A*, 2000, **281**(1–2), p 132–142.
47. A.V. Mamutov, S.F. Golovashchenko, N.M. Bessonov, V.S. Mamutov, Electrohydraulic Forming of Low Volume and Prototype Parts: Process Design and Practical Examples, *J. Manuf. Mater. Process.*, 2021, **5**(2), p 47.
48. B.M. Dariani, G.H. Liaghat, M. Gerdooei, Experimental Investigation of Sheet Metal Formability under Various Strain Rates, *Proc. Inst. Mech. Eng. Part B J. Eng. Manuf.*, 2009, **223**(6), p 703–712.
49. M. Rainforth, A. Patterson, A. Chamisa, A. *Rijkenberg, High Strength Steels for Light Weighting Automotive Applications*, n.d., https://www.sheffield.ac.uk/polopoly_fs/1.573534!/file/MRainforth.pdf
50. E. Cantergiani, C. Scott, B. Lawrence, C. Sinclair, 2015 T.C. Graham Prize Winner: High-Strength Interstitial-Free Steel Obtained Using FeC Amorphous Films and Induction Heating for Packaging Applications and Cladding with Lighter Metals for Car Body Panels, *Iron Steel Technol.*, 2016, **13**(1)